Journal of Materials Chemistry B

ROYAL SOCIETY OF CHEMISTRY

PAPER

View Article Online
View Journal | View Issue

Cite this: J. Mater. Chem. B, 2025, 13, 13992

Exploiting supercooled medium-chain lipids and surfactant combinations for solid-phase dominant nanostructured lipid carrier production

Daniel Sedough-Abbasian, Jiaming Mu, Jerin George Joseph, Gavin P. Andrews and Sheiliza Carmali *

Nanostructured lipid carriers (NLCs) are a promising delivery system for poorly water-soluble drugs, including lipophilic peptides. However, NLCs often display unpredictable drug partitioning between solid and liquid lipid phases, potentially compromising controlled release profiles. Here, we demonstrate a novel hybrid NLC approach that directs drug loading primarily to the solid phase while maintaining the structural advantages of established NLCs. Using cyclosporine A (CsA) as a model peptide, we exploited the significant solubility differential between medium-chain solid lipids (glyceryl caprylate: 338.95 ± 77.68 mg mL^{-1}; glyceryl caprate: 88.63 ± 8.80 mg mL^{-1}) and the liquid lipid component (soy liquid lecithin: 1.39 ± 0.09 mg mL^{-1}) to create a natural concentration gradient favouring a solid phase loading. By strategically combining these medium-chain lipids with selective surfactants, particularly PEG-100 stearate, we enabled the controlled transformation of initially supercooled melts into organised type I imperfect crystal structures that effectively encapsulate CsA within the solid lipid matrix. This approach allowed single-step hybrid NLC production at temperatures up to 20 °C lower than conventional methods while reducing homogenisation power requirements by 38%. Our optimised formulations maintained particle size (<200 nm), polydispersity (<0.3), and spherical morphology during four-week storage at 4 °C, room temperature, and 40 °C. Most notably, the controlled CsA release profiles in simulated intestinal fluid confirmed successful drug entrapment within the solid lipid matrix rather than the liquid phase. This work presents a robust strategy for producing stable, solid-phase dominant NLCs at reduced processing temperatures, with significant implications for controlled drug delivery and continuous manufacturing processes.

Received 24th March 2025,
Accepted 22nd September 2025

DOI: 10.1039/d5tb00676g

rsc.li/materials-b

Introduction

Lipid-based nanocarriers, now a thriving multi-million dollar market, are a key innovation in biodegradable drug delivery systems.[1] These versatile platforms effectively address the significant challenge of poor water solubility in approximately 90% of new chemical entities.[2] The advancement of these carriers, from conventional nano/micro emulsions and liposomes to more sophisticated self-emulsifying drug delivery systems, has dramatically improved drug bioavailability, exemplified by Novartis' commercial products Neoral® and Sandimmune® for cyclosporine A (CsA) delivery.[3–5] Despite these successes, the application of lipid-based delivery systems to a wider range of peptide therapeutics remains limited.[6]

The evolution of lipid nanocarrier design has led to more advanced systems, particularly solid lipid nanoparticles (SLNs) and nanostructured lipid carriers (NLCs).[7] SLNs, utilize solid lipids that exist as either solid matrices or supercooled melts,[8] with the latter representing a metastable liquid state where the lipid remains fluid below its melting point without crystallisation.[9] Similarly, NLCs, which combine solid and liquid lipids to create a less ordered matrix, can also exist in a metastable supercooled state, forming amorphous or "structureless" systems that impact drug encapsulation and release.[10]

While NLCs were initially designed to overcome SLN limitations by introducing imperfections in the crystal lattice through liquid lipid incorporation, they face the critical challenge of unpredictable drug partitioning between the solid and liquid phases.[10,11] This partitioning leads to variable drug release profiles, with molecules located in the liquid phase often displaying undesired burst release effects.[11] However, achieving predictable solid-phase drug loading remains elusive because no strategies exist to reliably direct drug partitioning between phases. Existing approaches have focused primarily on processing advantages rather than exploring how to create

School of Pharmacy, Queen's University Belfast, BT9 7BL Belfast, UK.
E-mail: s.carmali@qub.ac.uk

controlled solubility differences that could guide drug partitioning.[8,12]

To address this challenge, we concentrated on controlling the transition between type I (imperfect crystal) and type II (amorphous) structures.[13] type III NLCs, which contain multiple solid lipid compartments scattered throughout a liquid lipid matrix, were not investigated as our objective was to achieve solid-phase dominant drug loading through controlled crystallisation of a single solid lipid phase. The type I/type II transition provides the most direct pathway to transforming initially fluid, supercooled systems into organised crystal structures that effectively trap drugs in the solid component.

A significant barrier to implementing this structural control stems from the processing conditions required for production. Current methods rely on either low-energy solvent-based approaches or high-energy shear methods.[14,15] Although high-shear production offers scalable, solvent-free processing, commonly used long-chain lipids (12–22 carbons) like glyceryl dipalmitate/distearate and glyceryl monostearate require elevated processing temperatures (above 55 °C and 71.9 °C, respectively) to achieve the isotropic liquid state necessary for effective particle formation.[8,16–18] These high-temperature, multi-step processes risk peptide degradation and lead to significant drug loss through aqueous phase partitioning and particle aggregation from incomplete surfactant coverage.[19]

Recent studies suggest that lipid molecular structure, particularly chain length, could provide a solution to these processing challenges while enabling better control over drug distribution. Medium-chain lipids ($\leq$12 carbons) demonstrate unique phase behaviour, including enhanced supercooling tendency and lower melting temperatures.[8,12] For example, trilaurin (12 carbons) can be processed at just 43 °C with added supercooling stability.[8] This tendency for supercooling increases with decreasing chain length, offering an opportunity to fundamentally redesign the NLC production process while enabling directed drug partitioning through meticulous selection of lipid components with differential solubilisation capacities.

The stability, crystallisation behaviour, and drug distribution within these systems can be further controlled through strategic surfactant selection. Kuntsche and colleagues showed that different types of stabilisers significantly influence particle crystallisation, with complex patterns emerging based on the stabiliser system used.[20,21] Their work emphasised the importance of both stabiliser's molecular structure and its polar head groups in controlling particle behaviour.[12,21,22] These insights suggest that strategic surfactant selection and lipid combination could allow for controlled transformation of supercooled lipid matrices into stable nanostructures with desired properties, including directed drug partitioning towards the solid lipid phase. While medium-chain lipid properties[8,12] and surfactant-mediated crystallisation[20,21] have been studied independently, systematic exploitation of supercooling behaviour to control drug partitioning while reducing processing temperatures has received limited attention.

In this study, we demonstrate a novel hybrid NLC approach that harnesses a 243-fold difference in drug solubility between medium-chain solid lipids and the liquid lipid component to achieve solid-phase dominant drug loading. We selected cyclosporine A as our model peptide due to its well-characterised lipophilicity and thermal stability, and successful formulation in commercial lipid-based systems (Neoral® and Sandimmune®), providing established benchmarks while representing the target class of poorly water-soluble peptide therapeutics. Our systematic evaluation included surfactant combinations to control lipid crystallisation behaviour, comprehensive characterisation of particle properties, and stability assessment at 4 °C, room temperature and 40 °C. *In vitro* release studies under simulated physiological conditions confirmed peptide entrapment within the solid lipid matrix. This strategic lipid and surfactant selection enables single-step production at temperatures 20 °C lower than conventional methods while maintaining excellent formulation stability and controlled release characteristics.

Materials and methods

Materials

Glyceryl dipalmitate/distearate (Precirol® ATO 5), propylene glycol monocaprylate (Capryol® 90), propylene glycol dicaprylate/dicaprate (Labrafac® PG), polyglyceryl-3-esters of oleic acid (Plurol® Oleique CC 497) were kindly donated by Gattefossé (Lyon, France). Glyceryl caprate (Dermasoft® GMC MB) was kindly donated by Evonik (Essen, Germany) *via* Surfachem (Leeds, UK). Glyceryl caprylate (Lexgard® GMCY MB) were kindly donated by Inolex (Philadelphia, USA). PEG-100 stearate (Mrij® S100) was kindly donated by Croda (Snaith, England). Soy liquid lecithin was acquired from Fearn Natural Foods (Mequon, USA). Neoral® was obtained from Novartis (Basel, Switzerland). Cyclosporine A, sodium taurocholate hydrate 90%, lecithin soybean 90%, sodium chloride 99.5%, and *tert*-butyl methyl ether HPLC grade were purchased from Fisher Scientific (Leicestershire, UK). Polysorbate 80 (Tween® 80), sodium hydroxide, acetonitrile HPLC grade and malic acid were acquired from Sigma-Aldrich (Dorset, UK). Orthophosphoric acid 85% HPLC grade was acquired by Avantor (Leicestershire, UK). Captiva EMR lipid columns were purchased from Agilent (Cheshire, UK).

CsA-lipid solubility studies

Solubility in crystalline lipids. The solubility of CsA in glyceryl dipalmitate/distearate was determined using cross polarized microscopy.[23] Briefly, CsA (3 or 6 mg) was combined with glyceryl dipalmitate/distearate (300 μL) in a 500 μL microcentrifuge tube and mixed at 75 °C and 600 rpm for 2 days using an Eppendorf Thermomixer®. The mixture was then transferred to a 25 mm microscope slide and examined using an Olympus BX50® cross polarized microscope fitted with a Linkham THMS600® hot stage maintained at 85 °C. Following complete melting of the mixture, solid precipitates were observed using a 10× objective lens. CsA saturation solubility was determined by the presence of undissolved cyclosporine A crystals. All measurements were performed in triplicate (SI, Table S1).

Solubility in liquid and medium-chain solid lipids. For liquid and medium chain lipids, 300 μL of each lipid was accurately measured into a 500 μL microcentrifuge tube using a positive displacement pipette. Excess CsA was added incrementally, and the mixtures were stirred at 60 °C and 600 rpm (Eppendorf Thermomixer®) for a minimum of two days until visual solubilisation was achieved. Additional CsA was added as needed until saturation was observed. Saturated samples were then centrifuged at 40 °C for one hour at 10 000 rpm using an Axygen® Axyspin refrigerated microcentrifuge. A 10 μL aliquot of the supernatant was transferred to a 2 mL microcentrifuge tube and diluted appropriately for analysis (SI, Table S2). CsA concentration was determined using reverse-phase HPLC as detailed below. All measurements were performed in triplicate.

Preparation of CsA-loaded NLCs

Conventional two-step process (formulation F1). CsA-loaded NLC formulation F1 was prepared using a combined high-shear homogenisation and probe sonication process (Table 1). Initially, CsA (6.3 mg, 0.16% w/v) was dissolved in propylene glycol monocaprylate (47.4 μL) by stirring at 72 °C and 200 rpm for 7.5 minutes. Melted glyceryl dipalmitate/distearate (81.4 μL) was then added and mixed for another 7.5 minutes. Separately, an aqueous phase was prepared by dissolving surfactant 82 mg of polysorbate 80 or PEG 100 stearate in 4 mL of distilled water at 200 rpm. The lipid phase was heated to 10 °C above its melting point in a water bath before combining with the aqueous phase. The mixture was homogenised (Thermo Fisher PowerGen 500) at 12 333 rpm for 4 minutes, followed by probe sonication (40% amplitude, 5 seconds on/off pulses) for 10 minutes. The final formulation was cooled in an ice bath while stirring at 200 rpm for 10 minutes before storage.

Single-step process (formulations F2–F5). Formulations F2–F5 were prepared using a simplified single-homogenisation process (Table 1). The lipid phase was prepared by mixing CsA (6.3 mg, 0.42% w/v) with either glyceryl caprylate (C8) or glyceryl caprate (C10) (71.1 μL) at 200 rpm for 7.5 minutes at 10 °C above the lipid's melting point (SI, Table S2). Soy liquid lecithin (47.4 μL) was then incorporated with continued mixing for 7.5 minutes. In parallel, surfactant (45 mg of polysorbate 80 or PEG-100 stearate) was dissolved in 1.5 mL of distilled water at 200 rpm. The lipid phase was heated to either 52 °C (F2/F3) or 60 °C (F4/F5) before combining with the aqueous phase. The mixture was homogenised at 6800 rpm for either 2.5 minutes (F2/F3) or 7.5 minutes (F4/F5). The final formulations were cooled in an ice bath while stirring at 200 rpm for 10 min before storage. For all formulations, CsA content was maintained constant regardless of lipid solubility for comparative analysis.

All formulations (F1–F5) were prepared using multiple ($n \geq 2$) independent batches to ensure reproducibility, with batch-to-batch variability assessed for key parameters, including physicochemical and encapsulation properties.

Characterisation of CsA-loaded NLCs

Measurement of particle size, size distribution and surface charge. NLC particle size, polydispersity, and zeta potential were measured at 20 °C by dynamic light scattering (DLS) using a Zetasizer Nano ZS (Malvern Instruments Ltd, Malvern, UK). F1 was diluted 1 : 3 with distilled water while F2–F5 formulations were diluted 1 : 20. All samples were filtered with 0.45 μm hydrophilic polytetrafluoroethylene (PTFE) membrane filter. A refractive index of 1.462 and 20 °C was used to measure particle size and dispersity. Zeta potential was measured by laser Doppler micro-electrophoresis using a Zetasizer Nano ZS (Malvern Instruments Ltd, Malvern, UK). All analyses were conducted in triplicate for each formulation, and the mean and standard deviation calculated for each measured parameter.

Encapsulation efficiency (EE) and drug loading (DL). NLC samples (2 mL aliquots) were centrifuged at 4 °C and 10 000 rpm for 1 hour using an Axygen® Axyspin refrigerated microcentrifuge. After centrifugation, 500 μL of supernatant was collected and diluted with 1 mL of acetonitrile. The mixture was homogenised at 600 rpm using an Eppendorf Thermomixer® until complete dissolution. Samples were purified using an Agilent Captiva EMR lipid column, followed by a second wash with acetonitrile : water (80 : 20, 300 μL) to ensure complete CsA extraction.

CsA content was determined by reverse-phase HPLC. Encapsulation efficiency and drug loading were calculated using eqn (1) and (2), respectively,[24] where CsA_{Total} represents the total amount of CsA added to the formulation, and CsA_{Free} the amount of free (unentrapped) CsA detected in the supernatant after centrifugation. Drug loading was calculated as the percentage of CsA weight relative to the total weight of the solid content (CsA + lipids). All analyses were performed in triplicate.

$$\mathrm{EE}, \% = \frac{\mathrm{CsA}_{\mathrm{Total}} - \mathrm{CsA}_{\mathrm{Free}}}{\mathrm{CsA}_{\mathrm{Total}}} \times 100 \quad (1)$$

$$\mathrm{DL}, \% = \frac{\mathrm{CsA}_{\mathrm{Total}} - \mathrm{CsA}_{\mathrm{Free}}}{\mathrm{Solid\ content}_{\mathrm{Total}}} \times 100 \quad (2)$$

Homogenisation efficiency (HE). The recovery of CsA during NLC production was determined by combining 1.5 mL of the

Table 1 Composition of NLC formulations prepared in this study

	Solid lipid	Liquid lipid	Surfactant
F1	Glyceryl distearate/dipalmitate (C16/C18)	Propylene glycol monocaprylate	Polysorbate 80
F2	Glyceryl caprylate (C8)	Soy liquid lecithin	Polysorbate 80
F3	Glyceryl caprylate (C8)		PEG-100 stearate
F4	Glyceryl caprate (C10)		Polysorbate 80
F5	Glyceryl caprate (C10)		PEG-100 stearate

NLC formulation with 3 mL of the homogeniser wash in a 25 mL volumetric flask. The volume was made up to mark with acetonitrile and mixed at 200 rpm for 2 days. Afterwards, a 2 mL sample aliquot was purified using an Agilent Captiva EMR lipid column, with acetonitrile: water (80 : 20, 400 μL) as the secondary wash solution to ensure complete CsA extraction.

CsA content was determined by reverse-phase HPLC, and homogenisation efficiency was calculated using eqn (3), which represents the total drug recovery from the manufacturing process including both the final formulation and equipment wash. All analyses were performed in triplicate.

$$\mathrm{HE},\% = \frac{\mathrm{CsA}_{\mathrm{recovery}}}{\mathrm{CsA}_{\mathrm{Total}}} \times 100 \quad (3)$$

Cross-polarised light microscopy. An Olympus BX50® cross polarized microscope was used to visualize NLC formulations. All images were viewed using a 100× objective and Pixellink camera software was employed for image capture. NLC sample (50 μL) was spread onto a rectangular microscope slide and a circular 19 mm microscope slide placed on top of the sample. Twenty microlitres of immersion fluid were placed on top of the circular slide prior to observation. All analyses were performed in triplicate.

Differential scanning calorimetry (DSC). NLC samples used for DSC analysis were lyophilised using an Edwards Modulyo freeze dryer. The mass (mg) of empty and sample-containing DSC aluminium pans was weighed and recorded, after which they were placed on the TA Q20 DSC. Each pan was kept isothermal at −20 °C for 10 min, before a 5 °C min^{-1} ramp to 120 °C followed by descent at 5 °C min^{-1} to −20 °C. Thermal transitions, including melting points, crystallisation temperatures, and enthalpies were analysed using OriginPro 2021 (OriginLab Corporation, Northampton, MA, USA).

Powder X-ray diffraction (pXRD). Lyophilized NLC samples were analysed using a Bruker advance D8 diffractometer equipped with a copper X-ray tube (Cu Kα radiation, λ = 1.5418 Å). Samples were mounted on polymethyl methacrylate specimen holders sample holders and analysed over a 2θ range of 5° to 75° with a step size of 0.02° and a scan rate of 2° min^{-1}. All measurements were performed at room temperature under ambient conditions.

Raw diffraction patterns were processed using OriginPro 2021 (OriginLab Corporation, Northampton, MA, USA). For visualisation and peak identification, data smoothing was applied using the Savitzky–Golay method with a 100-point window, followed by baseline subtraction using asymmetric least squares smoothing (asymmetric factor: 0.001, threshold: 0.05, smoothing factor: 4, iterations: 10). Both processed (with Savitzky–Golay smoothing) and raw (unprocessed) data are presented for comparison.

Crystalline organisation was assessed qualitatively by identifying characteristic reflections at 18.7° and 23.0° (2θ) in PEG-100 stearate formulations, confirming type I imperfect crystal formation. Relative crystallinity was estimated by comparing the integrated peak areas of crystalline reflections to the total diffraction pattern area.

Crystallite sizes were estimated using the Scherrer equation ($D = K\lambda/\beta\cos\theta$) applied specifically to the reflections at 18.7° and 23.0° (2θ). Peak fitting was performed using Gaussian functions after baseline correction and smoothing to enable accurate full width at half maximum (FWHM) determination. Note: Instrumental broadening correction was not applied in this analysis, and therefore the reported crystallite sizes represent apparent values that may underestimate true crystallite dimensions. These values represent coherent crystallite domain sizes within the lipid matrix, not overall particle dimensions.

All analyses were performed in triplicate using independent sample batches.

Reverse-phase HPLC. Cyclosporine A quantification was performed according to European Pharmacopoeia 2025 guidelines using an Agilent 1220 (Agilent Technologies, Palo Alto, USA) system. Chromatographic separation was achieved using a ZORBAX 300 Stablebond RP18-5 column (250 × 4.6 mm, 5 μm particle size). The mobile phase consisted of HPLC-grade water : acetonitrile : methyl *tert*-butyl ether : *ortho*-phosphoric acid (52 : 43 : 5 : 0.1) at a flow rate of 2 mL min^{-1}. Analysis was performed at 75 °C with UV detection at 220 nm and a 20 μL injection volume.

The HPLC method was validated using a calibration curve spanning 0.005–0.8 mg mL^{-1} CsA concentrations. Good linearity was achieved (adjusted R^2 = 0.999) with limits of detection and quantification of 0.03 mg mL^{-1} and 0.08 mg mL^{-1}, respectively. Statistical analysis was performed using Originlab 2021 (OriginLab Corporation, Northampton, MA, USA), and all samples were analysed in triplicate (SI, Fig. S2).

NLC *in vitro* release studies

Simulated intestinal conditions. Release studies under simulated intestinal conditions were conducted using a modified FASSIF V2.[25] Briefly, sodium taurocholate (188.2 mg), lecithin (12.9 mg), sodium chloride (401 mg), sodium hydroxide (139.2 mg), and malic acid (221.9 mg) were dissolved in 16 mL of distilled water. The pH was adjusted to 6.8 with 2 M NaOH and 1 M HCl, and the final buffer volume was made to 20 mL.

NLC samples (1.5 mL) with homogeniser wash (2.5 mL) were combined with 1 mL of buffer. For each pre-determined time point (0.5, 1, 3, 6 hours) three separate NLC batches were prepared. Sodium dodecyl sulphate (50 mg, 1% w/v) was added to each batch prior experiment start to maintain sink conditions. Samples were incubated at 37 with continuous agitation at 100 rpm in a Qsonica incubator shaker. Sample aliquots (2 mL) were collected at pre-determined time points and centrifuged (10 000 rpm, 4 °C, 1 hour) using an Axygen® Axyspin refrigerated microcentrifuge. After centrifugation, the supernatant (500 μL) was diluted with 1 mL of acetonitrile and mixed at 600 rpm using an Eppendorf Thermomixer®. Samples were purified using an Agilent Captiva EMR lipid column with acetonitrile : water (80 : 20, 300 μL) as secondary wash solution. Final samples were filtered through 0.45 μm hydrophilic PTFE membrane filters before reverse-phase HPLC analysis. All measurements were performed in triplicate using independent NLC batches.

NLC colloidal stability study

Formulations F3 and F5 were placed at room temperature (19 °C) away from direct sunlight, 4 °C or 40 °C (Genlab

MINO/18/SS oven set) and stored for four weeks. Samples from each storage condition were analysed at week 0, 2 and 4 for their particle characteristics and encapsulation efficiency as previously described. Microscope studies were completed after four weeks storage. Formulations stored at each storage condition were tested as three independent triplicates.

Statistical analysis

Data are presented as mean ± standard deviation (SD) from at least three independent experiments ($n \geq 3$). Statistical analyses were conducted using GraphPad Prism version 10.2.2 for Mac (GraphPad Software, Boston, MA, USA, **https://www.graphpad.com**). Statistical significance was set at $p < 0.05$, with significance levels indicated as: *$p < 0.05$, **$p < 0.01$, ***$p < 0.001$, and ****$p < 0.0001$.

Results and discussion

Our study aimed to develop a simplified process for producing hybrid NLCs with CsA preferentially loaded in the solid lipid phase while preserving the structural benefits of standard NLCs.

We systematically investigated how lipid molecular structure and surfactant selection influence both drug loading and crystallisation behaviour to achieve three key objectives: (i) establish optimal lipid–CsA interactions with a preferred solubilisation in the solid phase, (ii) develop a milder, single-step hybrid NLC production process, and (iii) control the transformation of supercooled matrices from type II amorphous to type I imperfect crystal structures through strategic surfactant selection, to entrap CsA within the solid lipid matrix. The following sections detail how each objective was achieved, beginning with our investigation of lipid–CsA interactions and their impact on directed drug partitioning.

Enhanced CsA solubilisation and directed partitioning through medium chain lipids

We first focused on understanding how lipid molecular structure influenced CsA solubilisation capacity and could create a solubility differential between lipid components to direct CsA to concentrate in the solid phase. We quantitatively determined CsA saturation solubility across lipids varying in physical state (solid or liquid), alkyl chain length (C8–C18), and hydrophobicity. This screening approach aimed to identify a composition that would ensure both high overall encapsulation efficiency and preferential partitioning within the solid lipid phase.

Medium chain lipids demonstrated superior solubilisation capacity, with glyceryl caprylate showing exceptional solubility (338.95 ± 77.68 mg mL^{-1}), with a 34-fold increase over crystalline lipids (Fig. 1). Propylene glycol monocaprylate (131.73 ± 25.73 mg mL^{-1}) and glyceryl caprate (88.63 ± 8.80 mg mL^{-1}) also showed significantly enhanced solubilisation (Fig. 1). In contrast, long-chain lipid glyceryl dipalmitate/distearate showed notably lower solubility, with peptide precipitation observed at 10 mg mL^{-1} (Fig. 1B and SI, Table S1).

Crucial to our hybrid NLC approach, soy liquid lecithin showed the lowest CsA solubility among the tested lipids (1.39 ± 0.09 mg mL^{-1}), which compared to medium-chain lipid glyceryl caprylate showed a solubility differential of approximately 243-fold.

We thus hypothesised that the inclusion of soy liquid lecithin with a medium-chain lipid would provide a thermodynamic force for preferential CsA loading into the solid lipid component.

The enhanced solubilisation capacity of medium-chain lipids correlates with their unique molecular organisation. While long-chain lipids (*e.g.*, C18 lipids) form thermally stable parallel dimer clusters resistant to dissociation, medium-chain

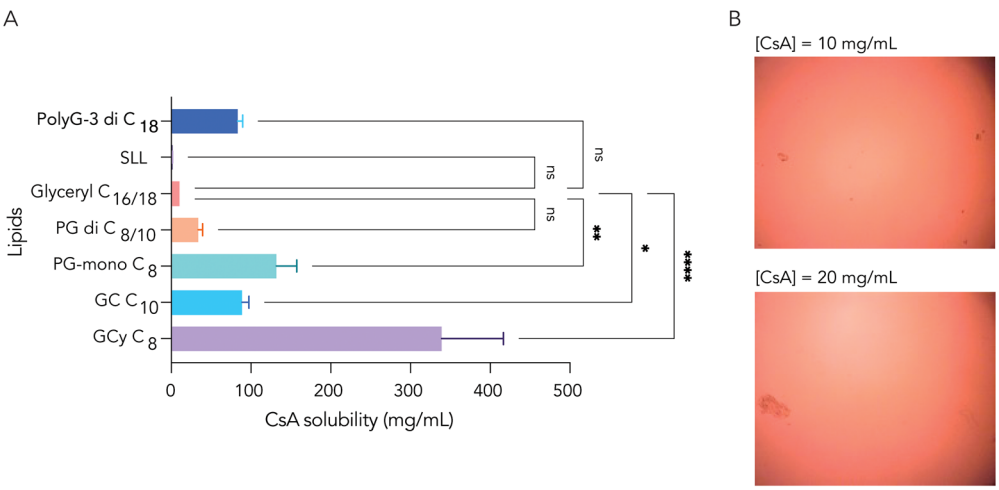

Fig. 1 (A) Saturation solubility of CsA in the various lipids tested in this study with (B) representative cross polarised microscope images of CsA (10 and 20 mg mL^{-1}) mixed with long-chain lipid glyceryl dipalmitate/distearate. GCy C_8 – glyceryl caprylate, GC_{10} – glyceryl caprate, PG-mono C_8 – propylene glycol monocaprylate, PG di $C_{8/10}$ – propylene glycol dicaprylate/dicaprate, glyceryl $C_{16/18}$ – glyceryl dipalmitate/distearate, SLL – soy liquid lecithin, PolyG-3 di C_{18} – polyglyceryl-3-esters of oleic acid. Values represent mean ± SD ($n = 3$). Results were analysed by one-way ANOVA, Dunnett's multiple comparisons test against glyceryl dipalmitate/stearate, and considered statistically significant when $p < 0.05$, with significance levels indicated as: * for $p < 0.05$, ** for $p < 0.01$, *** for $p < 0.001$ and ****$p < 0.0001$.

lipids adopt partially interdigitated clusters that readily monomerise at elevated temperatures.[26,27] This temperature-dependent structural flexibility allows for greater molecular mobility and more favourable drug–lipid interactions, Additionally, the shorter chain length of medium-chain lipids reduces steric hindrance during drug incorporation, potentially creating more accessible spaces for drug molecules within the lipid matrix.[28] The molecular-level advantages are reflected in the significantly higher solubility values observed for C8 and C10 lipids.

The low CsA solubility shown by soy liquid lecithin can be attributed to its high viscosity (>6 Pa s), which may impede molecular interactions, and its composition, with approximately 60% consisting of acetone-insoluble material.[29,30] While these characteristics may limit soy liquid lecithin's function as a solubiliser, it is ideally suited for our hybrid formulation strategy as a structural component that intrinsically directs CsA towards the medium-chain solid lipid phase.

Single-step process development using supercooled medium-chain lipids

Building on our solubility findings, we next investigated how the unique properties of medium-chain lipids could simplify the production of solid-phase dominant hybrid NLCs. The particle characteristics of the different formulations clearly demonstrate the advantages of our hybrid NLC approach (Table 2).

All formulations achieved sub-200 nm particle sizes suitable for drug delivery, with F2 and F3 showing particularly favourable characteristics (103.0 ± 19.0 and 98.2 + 0.54 nm, respectively). While these sizes are larger than commercial formulation Neoral® (28.3 ± 0.8 nm), our formulations showed better colloidal stability as indicated by their more negative zeta potentials (−44.7 to −56.9 mV compared to −6.6 ± 4.5 mV for Neoral®). The low polydispersity indices (<0.25) across all formulations confirmed uniform particle size distribution.

Notably, formulations F3 and F5 showed a 4-fold improvement in drug loading (3.73 ± 0.13% and 3.75 ± 0.52%, respectively) compared to conventional F1 formulation (Table 3). The moderate drug loading reflects our approach of maintaining peptide concentrations below saturation limits to ensure complete dissolution under processing temperatures and maintain long-term formulation stability. Moreover, obtained drug loading values were comparable to similar CsA and other peptide-loaded lipid systems.[24,31,32]

Table 2 Physical characteristics of NLC formulations including particle size, polydispersity index (PDI), and zeta potential. Data presented as mean ± SD. Commercial formulation Neoral included for comparison

	Average size (nm)	PDI	Zeta potential (mV)
F1	138.4 ± 8.7	0.18 ± 0.06	−30.9 ± 3.2
F2	103.0 ± 19.0	0.15 ± 0.07	−44.7 ± 4.7
F3	98.2 ± 0.54	0.25 ± 0.01	−51.3 ± 7.2
F4	169 ± 21	0.17 ± 0.06	−56.9 ± 8.9
F5	173.8 ± 6.05	0.21 ± 0.02	−51.3 ± 4.6
Neoral®	28.3 ± 0.8	0.1 ± 0.04	−6.6 ± 4.5

Table 3 NLC performance metrics, including homogenisation efficiency (HE), drug loading (DL), and encapsulation efficiency (EE)[a]

	HE (%)	DL (%)	EE (%)
F1	94.2 ± 6.6	0.94 ± 0.49	17.7 ± 9.9
F2	76.4 ± 4.8	—	—
F3	72.8 ± 3.4	3.73 ± 0.13	70.2 ± 1.0
F4	74.3 ± 6.3	—	—
F5	67.4 ± 4.3	3.75 ± 0.52	70.3 ± 8.7

[a] Drug loading and encapsulation efficiency were determined for formulations F3 and F5, which showed stable particle behaviour during centrifugation. Formulations F2 and F4 showed particle coalescence in the supernatant layer during centrifugation, preventing accurate quantification of free peptide content and reliable calculation of encapsulation parameters.

Medium-chain lipid formulations also showed a 2.5-fold greater lipid concentration compared to F1 (SI), allowing for more concentrated formulations with higher peptide content per unit volume, potentially offering manufacturing and dosing advantages.

While medium-chain lipid formulations showed somewhat lower homogenisation efficiency (67–76%) compared to long-chain lipid formulation F1 (94.2 ± 6.6%), this trade-off was offset by significant advantages in processing simplicity, drug loading capacity, and particle characteristics achieved through single-step production. Nanoparticle formation with glyceryl dipalmitate/distearate (F1) required a two-step process combining homogenisation with probe sonication, which led to lower lipid concentrations (28.4 mg mL^{-1}) and lower encapsulation efficiency (17.7 ± 9.9%).

In contrast, medium-chain lipid formulations (F2–F5) could form nanoparticles in a single step due to their larger melting/crystallisation temperature differences. This parameter ($\Delta M/C$), representing the difference between melting and crystallisation temperatures, indicates the supercooling window available for processing. Medium-chain lipids showed significantly larger $\Delta M/C$ values (glyceryl caprylate: 45.7 °C, glyceryl caprate: 36 °C) compared to glyceryl dipalmitate/distearate (5.5 °C; SI, Fig. S3). The processing advantage stems from the crystallisation behaviour of medium-chain lipids, which can be explained by Turnbull's equation for homogenous nucleation:

$$K_d = I \times V_d \quad (4)$$

where K_d represents the frequency of nucleation of supercooled droplets, I is the frequency of nucleation of the bulk liquid, and V_d is the droplet diameter.[33] The small $\Delta M/C$ of glyceryl dipalmitate/distearate leads to rapid nucleation, requiring additional processing steps to achieve surfactant integration before crystallisation occurs. Conversely, the extended crystallisation window of medium-chain lipids allows sufficient time for surfactant integration while maintaining controlled particle formation, as supercooled lipid systems demonstrate enhanced drug loading capacity compared to rapidly crystallising systems.[34]

The incorporation of soy liquid lecithin further enhanced this approach by enabling uniform nanoparticle formation at lower energy inputs.[35] Its anionic phospholipids and fatty acids

worked synergistically with the surfactants provide improved electrostatic stabilisation and low polydispersity. The high nanoparticle concentration achieved in a single process step created a "pearl-like network" of interconnected stabilising chains that prevents aggregation during storage, as the reduced available space limits particle velocity and Brownian motion.[10]

Controlled transformation of supercooled matrices through surfactant selection

Having established a viable single-step hybrid NLC production process, we next investigated how surfactant selection could control the structural organisation of these supercooled systems. Our goal was to transform initially amorphous type II matrices into more stable type I imperfect crystal structures while ensuring CsA entrapment within the solid lipid matrix.

DSC showed distinct surfactant-dependent thermal behaviour correlating with lipid matrix organisation (Fig. 2 and 3).

Polysorbate 80 and PEG-100 stearate systems showed fundamentally different lipid–surfactant interactions with corresponding implications for solid-phase drug entrapment.

Melting behaviour and matrix organisation. Melting thermographs in Fig. 2 showed that polysorbate 80 formulations had suppressed lipid crystallinity. F2 demonstrated complete suppression of characteristic lipid melting endotherms, with only surfactant-related thermal transitions detectable, indicating predominantly amorphous or supercooled liquid character.

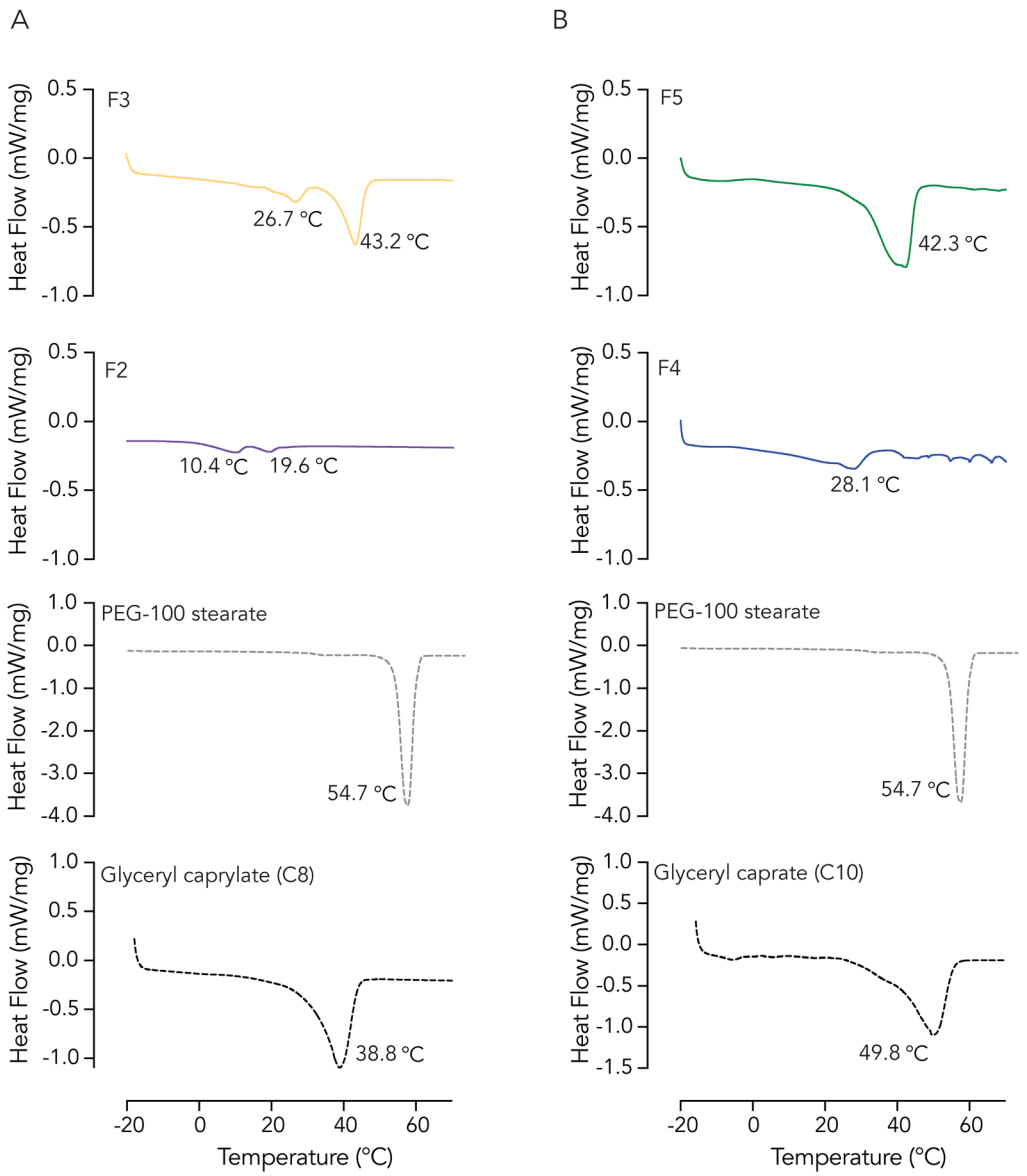

Fig. 2 DSC melting thermographs of medium-chain lipid NLCs showing surfactant-specific thermal behaviour. (A) C8-based and (B) C10-based formulations with PEG-100 stearate show organised melting transitions indicated co-crystallised complexes (F3: 43.2 °C, F5: 42.3 °C) and surfactant melting (F3: 26.7 °C) while polysorbate 80 formulations show suppressed lipid melting (F2: surfactant transitions only; F4: reduced melting at 28.1 °C). Individual components (bottom panels) provide reference transitions. Peak shifts and intensities demonstrate molecular interactions between lipids and PEG-100 stearate, confirming the presence of organised crystalline structures. Thermographs shown are representative from triplicate data.

F4 displayed a broad melting endotherm at 28.1 °C, substantially depressed from the crystalline glyceryl caprate melting point of 49.8 °C, suggesting the presence of mixed crystal phases or significant lattice defects.

PEG-100 stearate formulations demonstrated markedly different thermal behaviour, with F3 and F5 showing higher melting temperatures (43.2 and 42.3, respectively) and sharper endothermic transitions. The additional thermal event observed at 26.7 °C in F3 likely represents PEG-100 stearate chain melting or surfactant–lipid complex transitions. These elevated melting points indicate the formation of more ordered, co-crystallised structures between medium-chain lipids and PEG-100 stearate.

Crystallisation kinetics and nucleation control. Crystallisation thermographs provided complementary insights into nucleation control (Fig. 3). Polysorbate 80 formulations showed severely impaired crystallisation. F2 showed no detectable crystallisation exotherms, while F4 demonstrated extreme supercooling with crystallisation occurring at −12.1 °C. This behaviour is consistent with the formation of kinetically stable, supercooled liquid states, as reported for other medium-chain triglyceride systems stabilised with flexible surfactants.[36]

PEG-100 stearate formulations enabled controlled crystallisation at temperatures conducive to stable matrix formation. F3 crystallised at 22.6 °C, while F5 presented dual crystallisation events at 6.91 °C and 26.9 °C. The single crystallisation

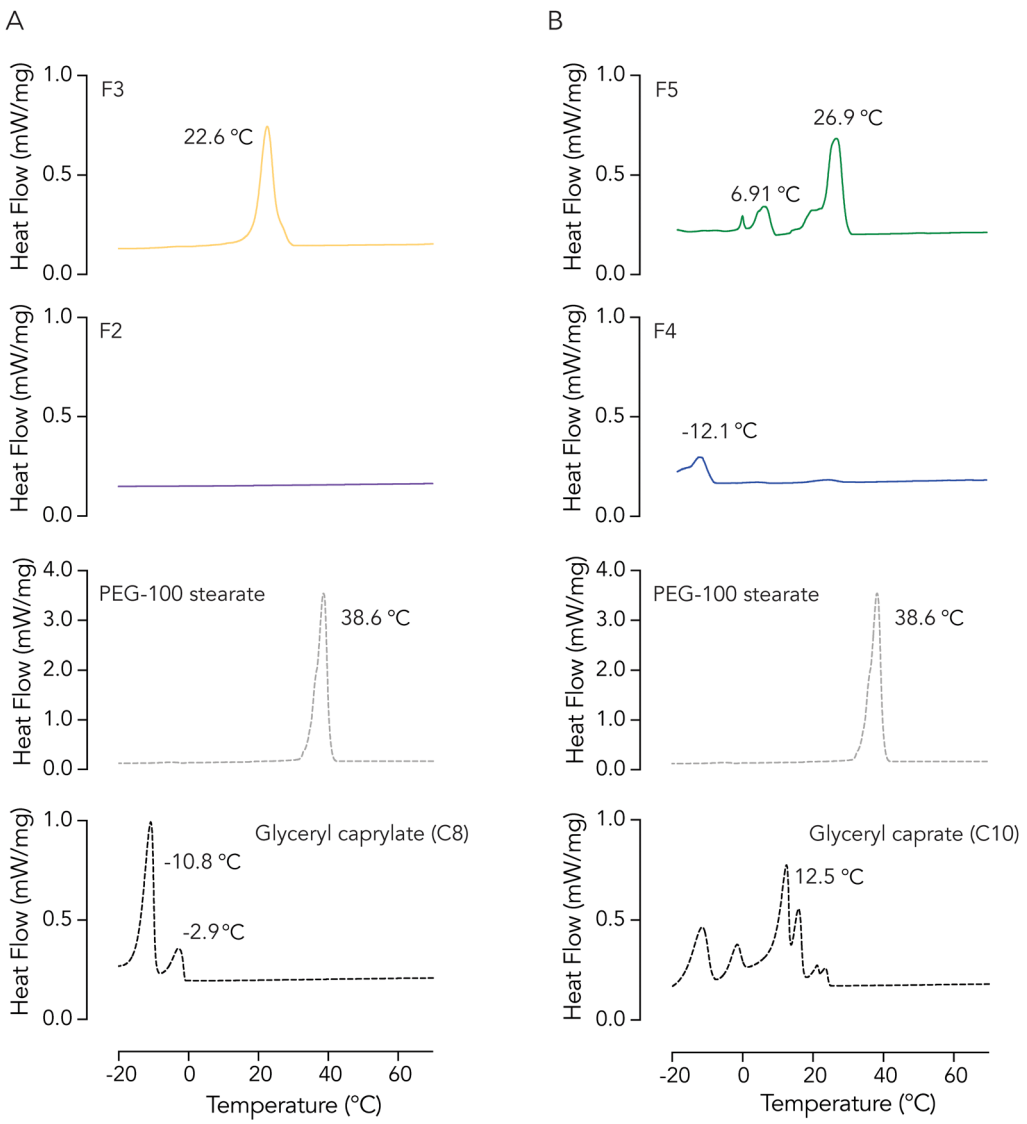

Fig. 3 DSC crystallisation thermographs demonstrating surfactant-mediated control of nucleation behaviour in medium-chain lipid NLCs. (A) C8-based formulations: F3 shows controlled crystallisation at 22.6 °C, while F2 shows no detectable crystallisation. (B) C10-based formulations: F5 shows dual crystallisation events (6.91 °C, 26.9 °C), while F4 shows severely suppressed crystallisation (−12.1 °C). Individual component analysis (bottom panels) reveals complex medium-chain lipid crystallisation behaviour and PEG-100 stearate nucleation template (38.6 °C). PEG-100 stearate promotes crystallisation above or near room temperature, while polysorbate 80 maintains supercooled stability, confirming surfactant-specific control over hybrid NLC structure formation. Thermographs representative of triplicate data.

event in F3 (C8 lipid) *versus* dual crystallisation in F5 (C10 lipid) suggests better integration of shorter chains with PEG-100 stearate, resulting in more uniform nucleation behaviour. Moreover, the dual crystallisation in F5 likely reflects sequential crystallisation of different lipid–surfactant assemblies. The higher temperature event (26.9 °C) corresponds to surfactant-templated arrangement of lipids in a stable β configuration, while the lower temperature event (6.91 °C) represents crystallisation of lipid α-subcell domains with reduced surfactant interaction, consistent with monoglyceride crystallisation behaviour.[37] Individual component analysis further supported PEG-100 stearate's role as a nucleation template, promoting organised lipid crystallisation, consistent with previous reports of PEG-stearate's ability to influence lipid structural organisation.[38]

Structural validation by powder X-ray diffraction. Powder X-ray diffraction analysis provided structural evidence supporting the thermal behaviour observations (Fig. 4). Polysorbate 80 formulations showed predominantly amorphous patterns; F2 presented broad, diffuse scattering with the lowest crystallinity (13.6 ± 7.1%), consistent with its complete absence of melting endotherms, while F4 showed moderate crystallinity (42.4 ± 1.7%) with multiple low-intensity peaks, explaining its substantial melting point depression.

PEG-100 stearate formulations showed sharp, well-defined diffraction peaks characteristic of organised crystalline structures. Characteristic reflections at 18.7° and 23.0° (2θ) confirmed type I imperfect crystal formation, providing structural validation for the higher melting temperatures and controlled crystallisation behaviour observed by DSC.

Mechanistic basis for surfactant control. These distinct thermal behaviours arise from fundamental differences in surfactant architecture. PEG-100 stearate, with its high melting point (>50 °C) and long saturated alkyl chain (C18) can act as a crystallisation template,[39] promoting heterogenous nucleation through co-crystallisation with medium-chain lipids. This creates organised interfacial domains that facilitate controlled solidification into type I imperfect crystal structures.

Conversely, polysorbate 80's lower melting point and flexible polyoxyethylene chains disrupts ordered lipid packing, maintaining predominantly amorphous or supercooled states. The inability of polysorbate 80 to promote crystallisation may also be related to its chain architecture, as shorter or more flexible ethylene oxide chains are known to inhibit crystallisation.[40] While kinetically stable, these type II amorphous structures lack the organised solid lipid domains necessary for controlled release and can potentially lead to burst release from liquid-phase drug loading.

The superior thermal organisation achieved with PEG-100 stearate directly translated to enhanced peptide encapsulation performance (Table 3). Medium-chain lipid formulations demonstrated substantially higher encapsulation efficiencies (F3: 70.2 ± 1.0%, F5: 70.3 ± 8.7%) compared to the conventional long-chain system (F1: 17.7 ± 9.9%). This 4-fold improvement in EE can be attributed to the extended supercooling window of medium-chain lipids, which maintains the lipid matrix in a fluid state during processing, facilitating optimal

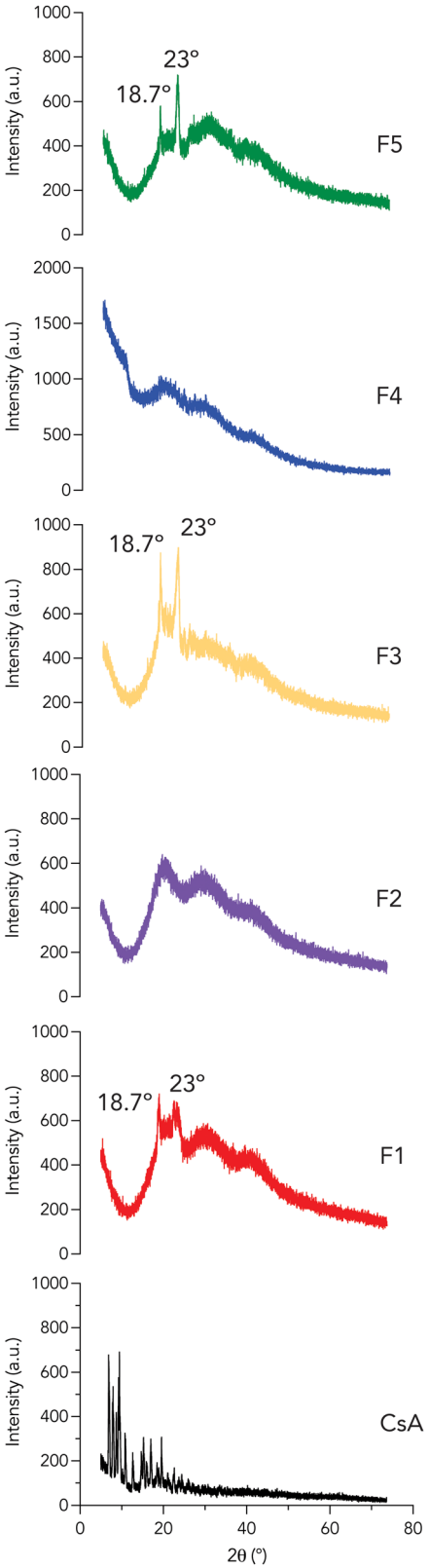

Fig. 4 Powder X-ray diffraction patterns demonstrating surfactant-controlled crystallisation in NLC formulations (raw, unprocessed data). Diffraction data showing characteristic crystalline reflections at 18.7° and 23.0° (2θ) in PEG-100 stearate formulations (F1/F3) *versus* minimal crystalline organisation in polysorbate 80 formulations (F2/F4).

peptide incorporation before crystallisation occurs. In contrast, the rapid crystallisation of long-chain lipids (small $\Delta M/C$ = 5.5 °C) provides insufficient time for complete peptide integration, resulting in expulsion or poor encapsulation efficiency, consistent with previous reports showing higher drug loading capacity in supercooled lipid systems compared to rapidly crystallising matrices.[34]

These structural findings have direct implications for CsA distribution in our hybrid NLCs. The organised type I crystalline matrices achieved with PEG-100 stearate, combined with the 234-fold solubility differential between medium-chain lipids and soy liquid lecithin, create optimal conditions for solid-phase drug entrapment and controlled release. This contrasts with previous cholesterol ester-based systems where fatty acid-containing stabilisers typically promoted crystallisation and polymeric stabilisers enhanced supercooled stability.[20,35]

Impact of structural transformation on stability and release properties

The mechanistic insights demonstrating how PEG-100 stearate enables controlled transformation of supercooled melts into organised type I crystal structures provide the foundation for understanding the practical performance of our hybrid NLC approach.

To validate the functional advantages of solid-phase dominant drug loading, formulations F3 and F5 were selected for comprehensive evaluation of long-term stability and *in vitro* release characteristics under simulated physiological conditions.

Colloidal stability. Both formulations maintained their spherical morphology across all storage conditions during the 4-week study period (SI, Fig. S4). Dynamic light scattering analysis confirmed excellent colloidal stability characteristics for both formulations, with polydispersity indices below 0.3 and particle sizes under 200 nm maintained across all tested conditions (Fig. 5). Formulation F3, containing glyceryl caprylate (C8), demonstrated superior stability characteristics, maintaining consistent particle sizes around 100 nm at both 4 °C and room temperature.

At elevated temperature (40 °C), F3 showed some variation but remained within acceptable pharmaceutical parameters (sub-200 nm range). This physical stability results from multiple complementary mechanisms: electrostatic repulsion from anionic soy liquid lecithin, steric stabilisation from PEG-100 stearate, and "pearl-like network" effect created by increased lipid concentration.[10,25]

Comparatively, formulation F5, containing the longer glyceryl caprate (C10), produced larger particles (150–175 nm) with greater size fluctuations at 4 °C and 40 °C storage conditions. These findings indicate that lipid chain length significantly influences hybrid NLC stability, with shorter chain glyceryl caprylate offering superior overall colloidal stability, likely

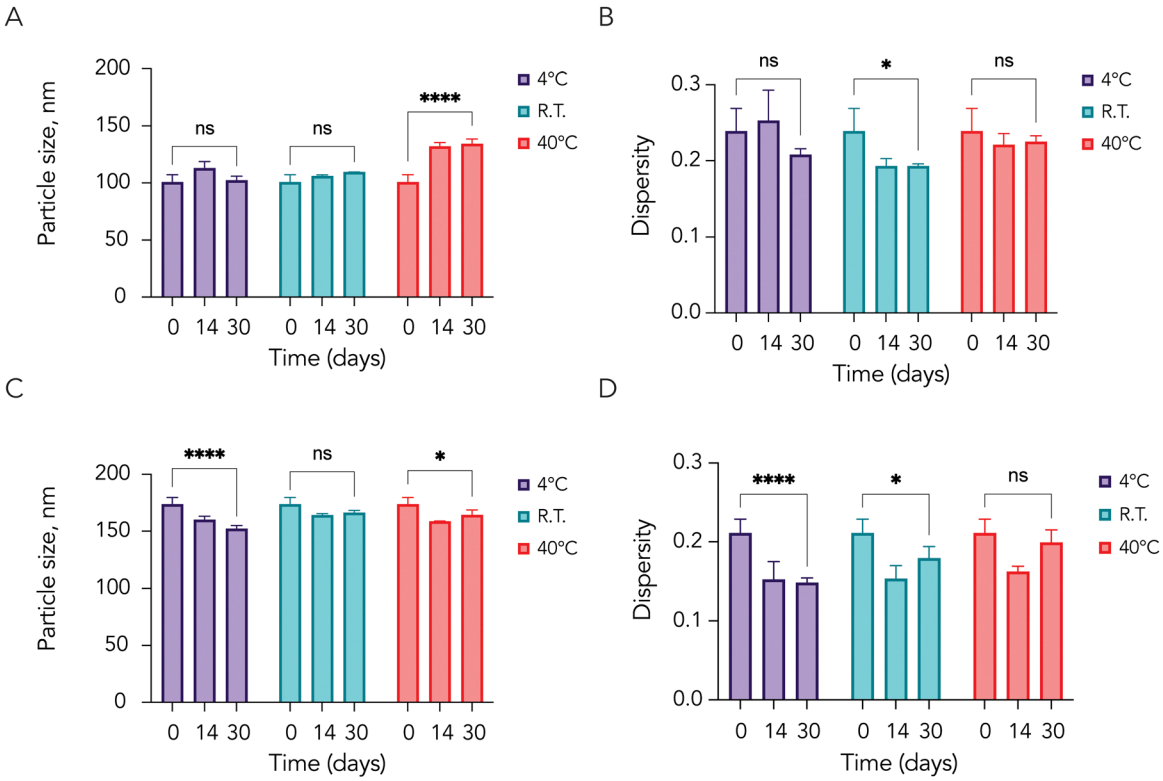

Fig. 5 Effect of storage time and temperature on particle characteristics of NLC formulations F3 (panels (A) and (B)) and F5 (panels (C) and (D)). Particle size (A) and (C) and polydispersity index (B) and (D) were measured at 0, 14, and 30 days under three storage conditions: 4 (purple), room temperature (cyan), and 40 (red). Statistical analysis performed using two-way ANOVA with Dunnett's multiple comparisons test comparing day 14 and day 30 to baseline (day 0) for each temperature condition and considered statistically significant when $p < 0.05$, with significance levels indicated as: * for $p < 0.05$, ** for $p < 0.01$, *** for $p < 0.001$ and **** $p < 0.0001$.

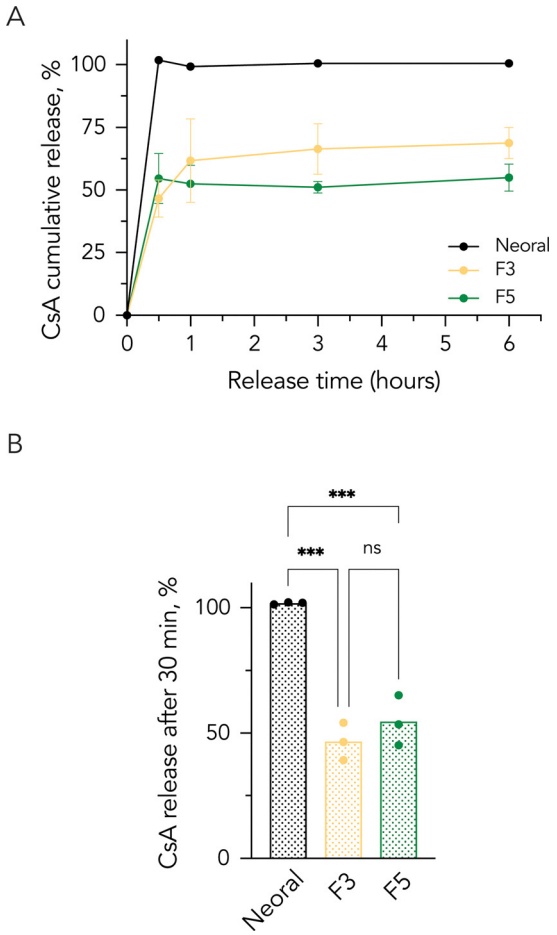

Fig. 6 (A) *In vitro* CsA release profiles from NLC formulations F3, F5 and Neoral in simulated intestinal fluid. Note: in Neoral, error bars are smaller than symbol used. (B) Comparison of CsA release between formulations F3, F5 and Neoral after 30 minutes of incubation at pH 6.8. Results were analysed by one-way ANOVA, Tukey's multiple comparisons test. Data was considered statistically significant when $p < 0.05$, with significance levels indicated as: * for $p < 0.05$, ** for $p < 0.01$, *** for $p < 0.001$ and ****$p < 0.0001$.

due to enhanced supercooling tendency and better integration with the surfactant system.

Storage temperature effects on CsA retention showed that refrigerated storage reduced encapsulation efficiency by 20–25% after 4 weeks, while room temperature and 40 °C storage maintained drug retention (SI, Fig. S4B). This temperature-dependent behaviour aligns with CsA's inverse solubility-temperature relationship in water (101.5 μg ml^{-1} at 5 °C, 32.95 μg ml^{-1} at 20 °C and 7.3 μg ml^{-1} at 35 °C),[41] where cold storage promotes increased peptide partitioning into the aqueous phase.[42,43]

***In vitro* release performance: evidence for solid-phase dominant loading.** Release studies under simulated intestinal conditions (Fig. 6) provided compelling validation of our solid-phase dominant hybrid NLC concept. Results demonstrated a fundamental shift from liquid-phase to solid-phase drug loading compared to conventional lipid-based delivery systems.

Neoral® demonstrated the expected immediate release characteristics typical of microemulsion systems, with complete drug release within 30 minutes. This rapid release reflects the drug's location within the readily accessible liquid phase of the microemulsion. In contrast, both hybrid NLC formulations (F3: 68.8 ± 6.3%; F5: 54.9 ± 5.4%) showed sustained release over 6 hours with reduced burst release effects. This controlled release behaviour, consistent across both medium-chain lipid types, further confirms preferential peptide entrapment within organised solid lipid matrices rather than liquid components.

These release characteristics confirm that our dual-control strategy successfully overcomes the main challenge of unpredictable drug partitioning in traditional NLCs. By combining thermodynamic driving forces with kinetic crystallisation control, we have demonstrated a pathway to predictable, solid-phase dominant peptide delivery systems. This hybrid approach not only enables single-step production at reduced temperatures but also provides the structural predictability necessary for controlled drug release, addressing key limitations that have hindered wider adoption of lipid-based carriers for peptide therapeutics. The successful integration of medium-chain lipid solubility differentials with surfactant-mediated crystallisation control establishes a robust platform for developing next-generation NLC formulations with enhanced therapeutic performance.

Conclusions

This study advances lipid-based carrier development through a novel hybrid NLC approach. By exploiting the significant solubility differential between medium-chain lipids and soy liquid lecithin, we created a thermodynamic driving force favouring solid-phase partitioning, combining the controlled release advantages of SLNs with the enhanced loading capacity and stability of established NLCs.

Our systematic investigation of lipid structure–property relationships and strategic surfactant selection enabled the production of these solid-phase dominant hybrid NLCs at temperatures up to 20 °C lower than conventional methods, with 38% less homogenisation power and elimination of ultrasonication steps. The combination of soy liquid lecithin for single-step nanoparticle formation and PEG-100 stearate for controlled crystallisation promoted the transformation from type II amorphous to type I imperfect crystal structures, providing a robust framework for ensuring peptide entrapment within the solid lipid matrix.

Our optimised formulations maintained particle sizes below 200 nm and showed consistent stability across various storage conditions (4 °C, room temperature, and 40 °C) over four weeks. Most notably, the reduction in burst release effects in simulated intestinal environments indicated successful drug partitioning within the solid lipid matrix, providing compelling evidence for our solid-phase dominant hybrid NLC approach.

This work establishes medium-chain supercooled melts as viable candidates for simplified, energy-efficient production of solid-phase dominant hybrid NLCs. The demonstrated ability to control crystallisation and peptide distribution through strategic lipid and surfactant selection, coupled with the

single-step manufacturing process, provides a promising platform for developing lipid-based delivery systems with enhanced control over drug release profiles. This approach holds significant implications for thermosensitive peptide delivery and continuous manufacturing processes, while further structural characterisation studies could provide additional mechanistic insight to further optimise this platform technology.

Author contributions

Conceptualisation: S. C., G. P. A., and D. S. A.; data curation: D. S. A., J. M., and J. G. J.; data analysis and interpretation: S. C., and D. S. A.; manuscript writing – editing and visualisation: S. C., and D. S. A.

Conflicts of interest

There are no conflicts to declare.

Data availability

Data for this article has been deposited in the Queen's University Belfast repository – Queen's University Research Portal at **https://pure.qub.ac.uk/**.

Supplementary information (SI), including details of lipid solubility screening, physicochemical characterisation, X-ray diffraction analysis, analytical method validation, thermal analysis, stability studies, and formulation calculations for all NLC systems, is available. See DOI: **https://doi.org/10.1039/d5tb00676g**.

Acknowledgements

This work was supported by the Department for the Economy (DfE) through a postgraduate studentship.

References

1 M. Intelligence, Lipid nanoparticles market growth, trends, COVID-19 impact and forecasts (2023–2030), 2023.
2 S. P. N. Bukke, C. Venkatesh, S. B. Rajanna, T. S. Saraswathi, P. K. Kusuma, N. Goruntla, N. Balasuramanyam and S. Munishamireddy, *Discover. Appl. Sci.*, 2024, **6**, 279.
3 P. Mohite, S. Singh, A. Pawar, A. Sangale and B. G. Prajapati, *Front. Drug Delivery*, 2023, **3**, 1232012.
4 N. Parquet, O. Reigneau, H. Humbert, M. Guignard, P. Ribaud, G. Socié, A. Devergie, H. Espérou and E. Gluckman, *Bone Marrow Transplant.*, 2000, **25**, 965–968.
5 D. B. Warren, S. Haque, M. P. McInerney, K. M. Corbett, E. Kastrati, L. Ford, H. D. Williams, V. Jannin, H. Benameur, C. J. H. Porter, D. K. Chalmers and C. W. Pouton, *Pharm. Res.*, 2021, **38**, 1531–1547.
6 A. L. Smart, S. Gaisford and A. W. Basit, *Expert Opin. Drug Delivery*, 2014, **11**, 1323–1335.
7 M. C. Teixeira, C. Carbone and E. B. Souto, *Prog. Lipid Res.*, 2017, **68**, 1–11.
8 K. Westesen and H. Bunjes, *Int. J. Pharm.*, 1995, **115**, 129–131.
9 H. Bunjes, B. Siekmann and K. Westesen, in *Submicron Emulsions in Drug Targeting and Delivery*, ed. S. Benita, CRC Press, London, 2019, pp. 175–204.
10 R. H. Müller, M. Radtke and S. A. Wissing, *Int. J. Pharm.*, 2002, **242**, 121–128.
11 A. Gordillo-Galeano, A. Ponce and C. E. Mora-Huertas, *J. Drug Delivery Sci. Technol.*, 2022, **76**, 103768.
12 M. A. Stahl, F. L. Lüdtke, R. Grimaldi, M. L. Gigante and A. P. B. Ribeiro, *Food Res. Int.*, 2024, **176**, 113821.
13 J. Mall, N. Naseem, Md. F. Haider, M. A. Rahman, S. Khan and S. N. Siddiqui, *Intell. Pharm.*, 2024, **3**, 243–255.
14 H. Patil, V. Kulkarni, S. Majumdar and M. A. Repka, *Int. J. Pharm.*, 2014, **471**, 153–156.
15 S. V. Khairnar, P. Pagare, A. Thakre, A. R. Nambiar, V. Junnuthula, M. C. Abraham, P. Kolimi, D. Nyavanandi and S. Dyawanapelly, *Pharmaceutics*, 2022, **14**, 1886.
16 J. Kuntsche and H. Bunjes, *Eur. J. Pharm. Biopharm.*, 2007, **67**, 612–620.
17 C. Dumont, *OCL*, 2022, **29**, 1.
18 M. de, C. V. Queiroz and L. A. Muehlmann, *J. Nanotheranostics*, 2024, **5**, 188–211.
19 Y. Yang, A. Corona and M. A. Henson, *J. Colloid Interface Sci.*, 2012, **374**, 297–307.
20 J. Kuntsche, M. H. J. Koch, M. Drechsler and H. Bunjes, *Colloids Surf., B*, 2005, **44**, 25–35.
21 J. Kuntsche, M. H. J. Koch, F. Steiniger and H. Bunjes, *J. Colloid Interface Sci.*, 2010, **350**, 229–239.
22 H. Salminen, T. Helgason, S. Aulbach, B. Kristinsson, K. Kristbergsson and J. Weiss, *J. Colloid Interface Sci.*, 2014, **426**, 256–263.
23 K. Göke and H. Bunjes, *Int. J. Pharm.*, 2017, **529**, 617–628.
24 C. Dumont, S. Bourgeois, H. Fessi, P.-Y. Dugas and V. Jannin, *Int. J. Pharm.*, 2019, **565**, 409–418.
25 M. Leigh, B. Kloefer and M. Schaich, *Dissolution Technol.*, 2013, **20**, 44–50.
26 M. Ideyo, T. Masaya, M. Hideyuki and I. Makio, *Food Nutr. Sci.*, 2013, **04**, 25–32.
27 J. A. Noël, L. Kreplak, N. N. Getangama, J. R. de Bruyn and M. A. White, *J. Phys. Chem. B*, 2018, **122**, 12386–12395.
28 L. Huynh, J. Grant, J.-C. Leroux, P. Delmas and C. Allen, *Pharm. Res.*, 2008, **25**, 147–157.
29 K. Yoshie, S. Yada, S. Ando and K. Ishihara, *Colloids Surf., B*, 2020, **195**, 111215.
30 E. Butina, *Biosci. Biotechnol. Res. Commun.*, 2021, **14**, 1861–1870.
31 A. Essaghraoui, A. Belfkira, B. Hamdaoui, C. Nunes, S. A. C. Lima and S. Reis, *Nanomaterials*, 2019, **9**, 1204.
32 S. G. Lee, C. H. Kim, S. W. Sung, E. S. Lee, M. S. Goh, H. Y. Yoon, M. J. Kang, S. Lee and Y. W. Choi, *Int. J. Nanomed.*, 2018, **13**, 3263–3278.
33 D. Turnbull, *J. Chem. Phys.*, 1952, **20**, 411–424.
34 K. Westesen, H. Bunjes and M. H. J. Koch, *J. Controlled Release*, 1997, **48**, 223–236.
35 H. Salminen, T. Helgason, B. Kristinsson, K. Kristbergsson and J. Weiss, *Food Chem.*, 2013, **141**, 2934–2943.

36 D. Cholakova and N. Denkov, *Adv. Colloid Interface Sci.*, 2024, **323**, 103071.
37 A. Alfutimie, N. Al-Janabi, R. Curtis and G. J. T. Tiddy, *Colloids Surf., A*, 2016, **494**, 170–179.
38 X. Li, X. Lin, L. Zheng, L. Yu, F. Lv, Q. Zhang and W. Liu, *Colloids Surf., A*, 2008, **317**, 352–359.
39 H. Ryu, M. Sung, H. Baek, S. Lee, B. Seo, K. Shin, M. Noh, J. B. Lee and J. W. Kim, *Chem. Eng.*, 2024, **486**, 149701.
40 T. K. Lind, E. J. Nilsson, B. Wyler, D. Scherer, T. Skansberger, M. Morin, V. Kocherbitov and J. Engblom, *J. Colloid Interface Sci.*, 2021, **592**, 468–484.
41 G. Ismailos, C. Reppas, J. B. Dressman and P. Macheras, *J. Pharm. Pharmacol.*, 1991, **43**, 287–289.
42 R. H. Müller, C. Freitas, A. zur Mühlen and W. Mehnert, *Eur. J. Pharm. Sci.*, 1996, **4**, S75.
43 K. M. Rosenblatt and H. Bunjes, *Eur. J. Pharm. Biopharm.*, 2017, **117**, 49–59.